

# Demystifying the Nvidia Ampere Architecture through Microbenchmarking and Instruction-level Analysis

Hamdy Abdelkhalik

New Mexico State University New Mexico State University  
enghamdy@nmsu.edu

Yehia Arafa \*

New Mexico State University  
yarafa@nmsu.edu

Nandakishore Santhi

Los Alamos National Laboratory  
nsanthi@lanl.gov

Abdel-Hameed Badawy

New Mexico State University  
badawy@nmsu.edu

**Abstract**—Graphics processing units (GPUs) are now considered the leading hardware to accelerate general-purpose workloads such as AI, data analytics, and HPC. Over the last decade, researchers have focused on demystifying and evaluating the microarchitecture features of various GPU architectures beyond what vendors reveal. This line of work is necessary to understand the hardware better and build more efficient workloads and applications. Many works have studied the recent Nvidia architectures, such as Volta and Turing, comparing them to their successor, Ampere. However, some microarchitecture features, such as the clock cycles for the different instructions, have not been extensively studied for the Ampere architecture. In this paper, we study the clock cycles per instructions with various data types found in the instruction-set architecture (ISA) of Nvidia GPUs. Using microbenchmarks, we measure the clock cycles for PTX ISA instructions and their SASS ISA instructions counterpart. We further calculate the clock cycle needed to access each memory unit. We also demystify the new version of the tensor core unit found in the Ampere architecture by using the WMMA API and measuring its clock cycles per instruction and throughput for the different data types and input shapes. The results found in this work should guide software developers and hardware architects. Furthermore, the clock cycles per instructions are widely used by performance modeling simulators and tools to model and predict the performance of the hardware.

**Index Terms**—Instructions Latency, Tensor core throughput, PTX, SASS, Ampere.

## I. INTRODUCTION

Graphics processing units (GPUs) have significantly increased in accelerating general-purpose applications from neural networks to scientific computing. GPUs are now considered the main hardware component in any high-performance supercomputer. For instance, Meta built one of the fastest supercomputers based on Nvidia Ampere architecture GPUs (A100) [1], and they are extending it to be the most powerful supercomputer in the world by mid-2022. Besides, tens of the top500 supercomputers [2] are GPU-accelerated.

Nvidia provides a new architecture generation with updated features every two years with little micro-architecture information about these features, making it difficult to quantify. This raises the need to study the effect of new features on the performance of applications. Nvidia introduced the tensor core (TC) unit to accelerate deep neural networks with the

introduction of Volta. This version of TC operates on FP16 and FP32 precision operations. Ampere architectures added a sparsity feature and new data precisions for the TC such as Int8, Int4, FP64, bf16, and TF32. Usually, there is little information beyond what the vendors choose to reveal in their whitepapers, which raises the need to quantify these features. Thus, researchers try to explain and demystify the new features of each GPU generation [3]–[8]. However, some areas still have not been fully covered in the literature. In this work, we focus on demystifying the clock cycle latency at the granularity of the instructions in the Instruction-set architecture (ISA). Similar work has been proposed before. For instance, the authors in [9] adapted some microbenchmarks to demystify some hardware units such as the memory, the tensor cores, and the arithmetic units. However, they only calculated the latency for memories at the granularity of the warp and the block, not the instructions. In another work [10], the authors calculated the latencies for only the memory hierarchy of older generations.

This paper presents microbenchmark analyses to dissect the instruction clock cycles per instructions for the Nvidia Ampere GPU architecture [11]. The microbenchmarks presented in this work are based on *Parallel Thread Execution* (PTX) [12]. PTX is an intermediate representation between the high-level language (CUDA) and the assembly language (SASS). So, it is portable among different architectures. PTX is open-source and well documented. However, its instructions do not directly execute on the hardware. It has to be converted to another architecture-dependent ISA. SASS, in this case, is closed-source and compatible only within each architecture family. This paper shows how each PTX instruction is mapped to SASS instruction while measuring the clock cycles for both ISAs. Furthermore, we present the clock cycle needed to access each memory unit. The microbenchmarks are based on a previous work by Arafa *et al.* [13], which calculated the clock cycle latencies for various instructions on different Nvidia architectures. However, there are no such studies done on the Ampere architecture. We also show the clock cycles and throughput for tensor core instructions on different data types.

Measuring the instructions clock cycles helps predict performance by GPU modeling tools. For instance, Arafa *et al.*

\* Now with Qualcomm Technologies, Inc.

[18] showed that by adopting correct latency for the GPU instructions, their performance model can improve its prediction accuracy compared to the actual hardware. Furthermore, Andersch *et al.* [10] have proven the critical relationship between the latencies and the performance. This work is the first step in accurately modeling the Ampere GPU architecture.

The main **contributions** of this paper are as follows:

- We demystify the Nvidia Ampere [11] GPU architecture through microbenchmarking by measuring the clock cycles latency per instruction on different data types.
- We show the mapping of PTX instructions to the sass instructions while measuring the clock cycles for both.
- We calculate the Ampere architecture tensor cores instructions (*WMMA*) clock cycle latency and throughput while clarifying their PTX and SASS instructions.
- We measure the access latency of the different memory units inside the Ampere architecture.

## II. BACKGROUND

Unlike multi-core CPUs, which have several powerful processors, GPUs have tens of simple processors that can work simultaneously to perform a specific task efficiently. This is viable for many applications that require numerous work to be performed in parallel, such as artificial intelligence and scientific computing.

An Nvidia GPU consists of several streaming multiprocessors (SM). The number of SMs varies with the generation of the GPU. Older architectures, such as Kepler, have fewer SMs (15 or 24), while contemporary architectures, such as Ampere, have a more significant number (124). The computation resources inside the SMs also vary depending on the architecture generation. Each SM is divided into hundreds of small cores performing different operations. GPUs have different types of memory units. The global memory and L2 cache are shared with all SMs. Furthermore, it has L1 caches, which are private to each SM. Moreover, threads inside a block can communicate through the shared memory.

The need for GPUs in many essential fields nowadays forces the vendors to enhance their GPU architecture to provide better performance. NVIDIA provides a new architecture every two years. New architectures not only have new hardware units but also may contain new ISA that increases performance. For example, in the Ampere architecture, Nvidia introduced much enhancement in the tensor core unit, making it faster and run on larger matrices. Moreover, it introduced the new L2 cache residency control feature, which automatically manages data to keep or evict from the cache.

Although these features are well documented in the whitepaper and online review websites, there are little information on the microarchitecture and the instruction-level enhancements found in the recent Ampere architecture. This paper fills this gap by providing a detailed instruction-level characterization of the Ampere GPU's instruction-set architecture (ISA).

## III. RELATED WORK

Various work have been conducted to dissect every undisclosed microarchitecture characteristic of the GPU [7], [8], [13], [19]–[21] using microbenchmarks. Unlike the Nvidia Ampere architecture, the older architectures such as Kepler, Fermi, Volta, and Turing are heavily studied in the literature. Some focused on the instruction level [6], [13], while others focused on the hardware unit itself [20], [22], [23]. In this section, we present some of these works in more detail.

Wong *et al.* [6] was the first to introduce microbenchmarks to measure the latency and the throughput of different types of memories and instructions. In [9], the authors modified some microbenchmarks to isolate the GPU features and study each separately. They studied the effect of the number of warps and blocks on the throughput for the memory, arithmetic, and tensor cores operations. They calculated the latencies per block, not per instruction. Other works [7], [8], [24] calculated instructions and memory throughput and latencies for the Kepler, Volta, and Turing architectures. However, [24] added more details about energy consumption. In the same spirit, Mei *et al.* [20] presented a microbenchmark for calculating the throughput and latencies of different types of memory units on older architectures such as Fermi, Kepler, and Maxwell.

Other researchers focused on profiling the tensor core in Volta and Turing architectures [22], [25], [26]. Recently, Sun *et al.* [21] tried to dissect the tensor core in the Ampere architecture. The authors focused on investigating the matrix multiply-accumulate using the *MMA* API, which gets executed on the tensor cores. They did not provide results for the *WMMA* API. In [27], the authors demonstrated the mapping of the PTX to the SASS instructions for the tensor core operations. Fasi *et al.* [23] developed a microbenchmark to investigate the tensor core numerical behavior and proved that the tensor core supports the subnormal number.

While all the previous work presents good progress, none focused on the clock cycles latency for all data types of each instruction while demonstrating the PTX and SASS mapping for each instruction. Moreover, to the best of our knowledge, we are the first to investigate every *WMMA* Tensor Core instruction clock cycles and throughput with different data types for the Nvidia Ampere architecture. Finally, Our work can be easily extended for future architectures.

## IV. METHODOLOGY

In this section, we introduce the microbenchmark design details. Our work is based on extending the microbenchmark presented in [13] to calculate the clock cycles per instruction for the Nvidia Ampere (AI100) GPU. We modified the microbenchmark to calculate the latency for dependent and independent instructions. Furthermore, we extended the code to calculate the clock cycles latency for the different types of memory units and the tensor core instruction.

The microbenchmarks are directly written in PTX, a pseudo assembly intermediate and architecture-independent ISA across all Nvidia. However, writing directly in PTX ISA can be tricky since the compiler translates the PTX code

```

1  .visible .entry _Z3AddPi(
2      .param .u64 _Z3AddPi_param_0
3  )
4  {
5      .reg .b32 %r<100>;
6      .reg .b64 %rd<100>;
7
8      ld.param.u64 %rd1, [_Z3AddPi_param_0];
9      cvta.to.global.u64 %rd4, %rd1;
10
11     add.s32 %r5, 5, %r3;
12     add.s32 %r7, %r5, 2;
13     mov.u32 %r1, %clock;
14     add.u32 %r11, 6, %r7;
15     add.u32 %r12, %r5, 7;
16     add.u32 %r13, %r12, %r1;
17     mov.u32 %r2, %clock;
18     sub.s32 %r8, %r2, %r1;
19
20     st.global.u32 [%rd4], %r8;
21     st.global.u32 [%rd4 + 8], %r11;
22     st.global.u32 [%rd4 + 16], %r12;
23     st.global.u32 [%rd4 + 20], %r13;
24     ret;
25 }

```

Fig. 1. Computing unsigned add instruction latency.

```

1      mov.u64 %r19,%rd4;
2      mov.u64 %r40,0;
3  $Mem_store:
4      st.wt.global.u64 [%r19], %r19+8;
5      st.wt.global.u64 [%r19+8], %r19+16;
6      st.wt.global.u64 [%r19+16], %r19+24;
7      st.wt.global.u64 [%r19+24], %r19+32;
8      add.u64 %r19,%r19,32;
9      add.u64 %r40,%r40,32;
10     setp.lt.u64 %p1, %r40, 52268760;
11     @%p1 bra $Mem_store;
12
13     mov.u64 %r40,0;
14     mov.u64 %r1, %clock64;
15  $Mem_load:
16     ld.global.cv.u64 %r4, [%rd4];
17     ld.global.cv.u64 %r16, [%r4];
18     ld.global.cv.u64 %r17, [%r16];
19     ld.global.cv.u64 %r20, [%r17];
20     add.u64 %r40,%r40,32;
21     setp.lt.u64 %p1, %r40, 262144;
22     @%p1 bra $Mem_load;
23
24     mov.u64 %r2, %clock64;
25     sub.s64 %r7, %r2, %r1;

```

Fig. 2. Computing L2 cache and global memory access latency

```

1  //reading from shared memory
2  mov.u64 %r1, %clock64;
3  ld.shared.u64 %r25,[shMem1];
4  add.u64 %r40,%r25,32;
5  mov.u64 %r2, %clock64;
6
7  sub.s64 %r7, %r2, %r1;
8  add.u64 %r22, %r7, 10;
9
10 //storing to the shared memory
11 mov.u64 %r1, %clock64;
12 st.shared.u64 [shMem1],50;
13 add.u64 %r24,%r23,32;
14 mov.u64 %r2, %clock64;
15
16 sub.s64 %r16, %r2, %r1;
17 add.u64 %r22, %r16, 10;

```

Fig. 3. Computing device shared memory access latency.

into another architecture-dependent ISA, SASS. There is not much information available on how the compiler does the mapping from PTX to SASS. For instance, the compiler can optimize multiple PTX instructions into one SASS instruction. In order to overcome these limitations and ensure the proper instructions get executed are the ones we need, we dynamically read the SASS instruction trace at the run time of each PTX microbenchmark written. We use the *Tracing Tool* from *PPT-GPU* [17] to do that. We then tweak the PTX microbenchmark by trial and error to give us the correct SASS results.

#### A. Instructions Clock Cycles Latency

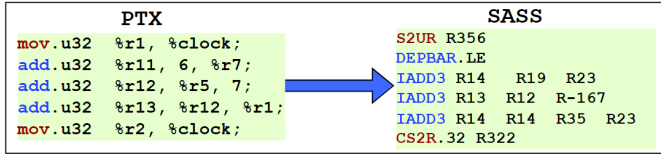
We used only one thread per block to measure the instruction latency. We have two steps. *First*, We run a code that calculates the clock cycles for the studied instruction with a specified data type. For instance, the code shown in Figure 1 calculates the latency of the add instruction where the operands are 32-bit registers. In general, measuring the latency can be performed by reading the clock before and after the instruction, as shown in Figure 1 lines 13 and 17. Then, we subtract the two clock readings (line 18) to

TABLE I  
THE RELATION BETWEEN THE NUMBER OF INSTRUCTIONS AND THE AVERAGE CYCLES FOR ADD.U32 INSTRUCTION

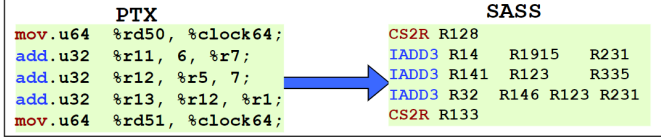
# instrs	CPI
1	5
2	3
3	2
4	2

calculate the difference or the required latency. We execute the three independent add instructions (lines 14-16). We also used dependent instructions and found that latency increased compared to independent instructions. Finally, we return the latency value to the main CUDA function and divide it by 3 to calculate the number of cycles for each instruction. We use 3 instructions to overcome the first launch overhead. We found that executing only one instruction will result in an unexpected higher number of cycles. Table I shows an example for *add.u32* instruction. The first instruction takes around 5 cycles. Nevertheless, when we use more than 3 instructions, the average number of cycles per instruction (CPI) is 2.

*Second*, we inspect the sass instruction using the dynamic *Tracing Tool* from *PPT-GPU* [18] to ensure that the mapping from PTX to SASS is correct and no additional overhead or instruction is added at runtime by the compiler. The PTX code shown in Figure 4(a) provides an inaccurate latency for the add instruction when storing the clock in 32-bit registers. The dynamic SASS instruction trace shows a barrier between the two clock readings, as shown in the second instruction of the SASS part. This barrier causes a considerable change in the results (around 33 cycles increase in this case). One method to overcome this barrier is to use the 64-bit registers to store the clocks, which remove the barrier and provide an accurate measurement, as shown in Figure 4(b). The CPI for the first



(a) Using 32 bit clocks register



(b) SASS 64 bit clocks register

Fig. 4. Mapping of PTX to SASS when using 32 and 64 bits clock registers

and second cases are 13 and 2 cycles, respectively. Finally, we calculate the clock overhead using two consecutive clock reading instructions and find that it equals 2 cycles.

### B. Memory Units Access Latency

To calculate **global, L2, and L1 cache memories latency**, we use a pointer chasing technique, in which each array elements are dependent on the previous ones. This technique forces the reading operations to be serialized to calculate the latency correctly. Otherwise, many reading operations can be issued simultaneously, which makes the latency measurements inaccurate. Figure 2 shows the PTX microbenchmark for the memory latency calculations. Line 1 moves the array address to the `%r19` register. Then, we start a counter with a zero value in the `%r40` register. This counter is used to iterate over the array of elements. Lines 3 and 9-11 represent the loop instructions. Lines 4 to 7 are used to store the array of elements in which each element is dependent on the previous one. After storing the results, we use the instructions from lines 14 to 24 to read the clocks while reading every element in the array. From 16 to 19, we have 4 load instructions to load 4 values, which are repeated to read all the array elements.

The `ld` instruction can be used with many operators such as `cv`, `ca`, and `cg`. Each operator has its usage. `ca` is used to cache on all available levels (global-L1-L2) while the `cg` caches only in L2. On the contrary, we use `cv` because it bypasses the caches, which we need when we calculate the global memory latency. We use 4 instructions because we found that in many cases, the compiler unrolls the loops by 4 when we inspected the dynamic trace of some Cuda applications that use loops. The difference between the global memory code and the L2 cache code is the operator used with the `ld` instruction and the number of the elements in the array. For the L2 cache, we use the `cg` operator, and the total size of the array elements must be less than the L2 size, while for the global memory code, it must be larger than the L2 cache to avoid L2 cache residency. Likewise, we repeat the same methodology with the `ca` operator to calculate the **L1 cache latency**.

For the **shared memory**, we load and store instructions between reading the clocks, as shown in lines 3-12 of Figure 3.

```

1 __global__ void wmma_example(atype *a, btype *b, ctype *c, dtype *d)
2 {
3     unsigned int start, start_time=0, end_time=0;
4     // Part 1: Declare the fragments
5     wmma::fragment<wmma::matrix_a, M, N, K, atype, LAYOUT_A> a_frag;
6     wmma::fragment<wmma::matrix_b, M, N, K, btype, LAYOUT_B> b_frag;
7     wmma::fragment<wmma::accumulator, M, N, K, ctype> c_frag;
8
9     // Part 2: loading the values from the memory
10    wmma::load_matrix_sync(a_frag, a, A_STRIDE);
11    wmma::load_matrix_sync(b_frag, b, B_STRIDE);
12    wmma::load_matrix_sync(c_frag, c, C_STRIDE, LAYOUT_C);
13
14    // Part 3: running the multiple+add on matrices
15    start_time=clock();
16    for (int i=0; i<iters*iters1; i++){
17        wmma::mma_sync(c_frag, a_frag, b_frag, c_frag);
18        wmma::mma_sync(c1_frag, a1_frag, b1_frag, c1_frag);
19        wmma::mma_sync(c2_frag, a2_frag, b2_frag, c2_frag);
20        wmma::mma_sync(c3_frag, a3_frag, b3_frag, c3_frag);
21    }
22    end_time=clock();
23
24    // Part 4: store the values from the memory
25    wmma::store_matrix_sync(d, c_frag, C_STRIDE, LAYOUT_C);
26
27    if (threadIdx.x==1)
28        printf("CLOCK for all=%d \t %d \n", ((end_time-start_time)-2)
29            /(4*iters1), tid);
30 }

```

Fig. 5. Computing the tensor core WMMA instruction clock cycles latency for U8 data type.

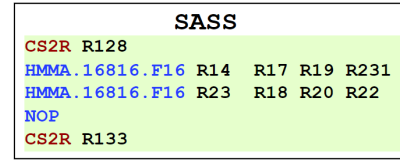


Fig. 6. SASS instructions of running one TC instruction

However, we needed to add another instruction that depends on the `ld` or `st` instructions to prevent the compiler from executing the clock reading instruction before finishing, as shown in lines 4-13.

### C. Tensor core Instructions Latency and Throughput

The Tensor core (TC) unit is a very trivial unit for accelerating machine learning applications. Each SM in the Ampere architecture contains 4 tensor cores that can run the multiple-add operation on 3 matrices in the form  $D=A*B+C$  where A, B are the inputs and C, D are the accumulators. Unlike the Volta, which supports only *fp16* precision for the inputs, the Ampere architecture supports many types, such as *FP16*, *bf16*, *tf32*, *f64*, *u8*, *u4* and the *single bit*. The general arithmetic instructions use one thread to execute and can communicate only through the global or shared memory. On the other hand, the TC instructions use all the 32 instructions in the dedicated warp. To demystify the Ampere architecture's TC instructions with the new data types, we designed a special microbenchmark is written in Cuda programming language. The microbenchmarks are inspired by Jia *et al.* [7] work, which focused on Volta architecture.

Some of the new data types that were introduced in the Ampere architecture are still in the experimental stage, as mentioned in PTX and CUDA documentation [28]. Moreover,

because each data type has its shapes, stride, and layout, we use a different function to calculate the latencies of each type. Figure 5 shows the code used to calculate the TC instruction latency of *U8* data type. Lines 5 to 7 create a fragment in which the registers are prepared to get the matrix elements to be stored. We create 4 fragments; however, we do not write all to make the shape smaller. Then, we load the data from memory (lines 10-12), and the same goes for the other fragments. As previously explained, we read the clocks before and after the TC WMMA execution (lines 15 to 22) and subtract them before printing, as shown in lines 28-29. From lines 16 to 21, we run 4 TC instructions (1 per TC) numerous times. We used 4 instructions because we found that calculating the latency from one TC with one instruction provides inaccurate measurement. For example, Figure 6 shows the dynamic SASS instructions of running one instruction on one TC. The NOP instructions refer to a warp synchronization in PTX, and we found that the latency here is not the same as mentioned in the white paper. This also happens when we run one instruction several times. Finally, we calculate the latency per instruction and print them by lines 28-29. A similar method is used to calculate the TC’s WMMA throughput.

## V. RESULTS

In this section, we present the detailed setup and results. We first show the instructions clock cycles latency. Next, we explain the memory access latencies. Finally, We present the Tensor Core latency and throughput. We run all the microbenchmarks on the Nvidia *Tesla A100* GPU.

### A. Instructions Latency

We found that dependency directly affects the instructions clock cycle latency. Hence, we rerun the microbenchmark with a sequence of dependent instructions (shown in Figure 1), replacing the dependent sequence with another sequence of independent instructions. Table II shows the CPI for dependent and independent sequences for some of the instructions. For instance, single precision add instruction shows 4 and 2 cycles, respectively. We also found that with no dependency, the 3 *add.u32* instructions mentioned in Figure 1 are mapped to the same sass instruction (*IADD*) as shown in Figure 4(a). Nevertheless, PTX instructions may be converted to different instructions when we use three dependent instructions. For example, the *add.u32* PTX instruction can be mapped to *IADD3* or *IMAD.IADD* with the dependency case.

Table V depicts the various PTX-SASS instructions with their measured clock cycles latencies. We have a separate PTX kernel (microbenchmark) for each field in the table.

Next, we discuss some additional insights we found while generating the results:

**1:** The *mad* instruction runs on the floating pipeline, not the integer pipeline, even if we use it with integer values. This can be proven by the following:

- The PTX instruction *mad.lo.u32* in Table V is mapped to the SASS *FFMA* (floating multiple-add).

TABLE II  
THE CPI FOR DEPENDENT AND INDEPENDENT INSTRUCTIONS

# instrs	CPI for dependent	CPI for independent
add.f16	3	2
add.u32	4	2
add.f64	5	4
mul.lo.u32	3	2
mad.rm.f32	4	2

- We created a special code that runs two add instructions and two mad instructions using one thread, and we found that the total number of cycles is around 4 cycles. This means that each one of the four instructions takes 1 cycle. It proves that each of the two types is executed simultaneously on different pipelines.

Showing that *mad* instruction uses another pipeline explains why the dependent PTX *add.u23* instruction is mapped to the SASS (*IMAD.IADD*) instruction in some cases. The compiler is trying to use the floating pipeline while waiting for the integer pipeline to commit.

**2:** Except for *bfind*, *min* and *max* instructions there is no difference in clock cycles or mapping between PTX to SASS when using a signed or an unsigned instruction. For instance, *add.u64* and *add.s64* provide the same mapping and the same latency.

**3:** Usually, a *mov* or *add* instruction is used to initialize a register with a value before using this register as an input operand to the instruction that we need to calculate its latency. However, in some cases, we found that the clock cycles and the PTX-SASS mapping change depending on how the inputs are initialized. For example, the PTX *neg.f32* is mapped to the SASS *FADD* when we use add instruction to initialize the inputs. on the other hand, it merges the *mov* and the *neg* instructions together in one SASS instruction (*IMAD.MOV.u32*) when we use *mov* for initializing. The same happens for the *abs.f32* instruction.

**4:** Although many PTX instructions have a 1-to-1 mapping to SASS, others such as *div*, *rem*, *sinf*, and *cosf* are translated to multiple different SASS instructions.

**5:** Not all instructions with the same data type have the same latency. More specifically, *mad.lo.u64* is mapped to an *IMAD* SASS instruction which takes only 2 cycles. However, the double precision add, sub and fma instructions take 4 cycles each.

**6:** For the *testp* instruction, the latency depends on the state.

### B. Memory Access Latencies

The observed latencies of the different types of memories are shown in Table IV. The global memory latency is around 290 cycles. This value does not include the cache misses latencies because we prevent caching at all levels. This number is improved compared to Turing architecture which is 434 cycles [13]. The L2 access latency is 200 cycles compared to 188 cycles for Turing architecture. Furthermore, the L1 cache hit for both Ampere and Turing architectures is 33 and 32

TABLE III  
THE TENSOR CORES LATENCIES AND THROUGHPUT

Supported shapes	Inputs	Accumulators	Cycles	Measured-theoretical	Instructions
m16n16k16 - m8n32k16 - m32n8k16	.f16	.f16	16	311-312 GB/s	PTX: <code>wmma.mma.sync.aligned.row.row.m16n16k16.f16.f16</code> SASS: <code>2*HMMA.16816.F16</code> – each inst. is 8 cycles
m16n16k16 - m8n32k16 - m32n8k16	.f16	.f32	16	310-312 GB/s	PTX: <code>wmma.mma.sync.aligned.row.row.m16n16k16.f16.f32</code> SASS: <code>2*HMMA.16816.F32</code> – each inst. is 8 cycles
m16n16k16 - m8n32k16 - m32n8k16	.bf16	.f32	16	310-312 GB/s	PTX: <code>wmma.mma.sync.aligned.row.row.m16n16k16.f32.bf16.bf16.f32</code> SASS: <code>2*HMMA.16816.F32.BF16</code> – each inst. is 8 cycles
m16n16k8	.tf32	.f32	16	132-156 GB/s	PTX: <code>wmma.mma.sync.aligned.row.row.m16n16k8.f32.tf32.tf32.f32</code> SASS: <code>4*HMMA.1684.F32.TF32</code> – each inst. is 4 cycles
m8n8k4	.f64	.f64	16	19-19.5 GB/s	PTX: <code>wmma.mma.sync.aligned.row.row.m8n8k4.f64.f64.f64.f64.rn</code> SASS: <code>1*DMMA.884</code> – each inst. is 16 cycles
m16n16k16 - m32n8k16 - m8n32k16	.u8	.u32	8	594-624 GB/s	PTX: <code>wmma.mma.sync.aligned.row.row.m16n16k16.s32.u8.u8.s32</code> SASS: <code>2*IMMA.16816.U8.U8</code> – each inst. is 4 cycles
m8n8k32	.u4	.u32	4	1229-1248 GB/s	PTX: <code>wmma.mma.sync.aligned.row.col.m8n8k32.s32.u4.u4.s32</code> SASS: <code>1*IMMA.8832.U4.U4</code> each inst. is 4 cycles

cycles, respectively. For the shared memory, we found that the store access latency takes a smaller value than the load instruction, 23 and 19 for load and store, respectively.

### C. Tensor Core Latencies and Throughput

The Ampere architecture ISA provides various SASS instructions that run on the Tensor Core, which supports the newly added data types. The Volta Architecture’s ISA has only the *HMMA.884* SASS instruction handles all Tensor Core operations (single and mixed-precision operations). For Turing, two kinds of the *HMMA* SASS instructions exist which runs on different input shapes, *HMMA.1688* and *HMMA.884* [26].

Table III depicts the Ampere architecture’s TC instructions. More specifically, *DMMA.884*, *IMMA.16816* and *IMMA.8832* were added to handle the FP64, U8 and U4 data types, respectively. Each PTX instruction of each data type is translated to a different number of SASS instructions. For the FP16 BF16 and U8 inputs, the PTX is translated to 2 instructions. The TensorFloat-32 (TF32) precision is mapped to 4 SASS instructions, while the FP64 and U4 are mapped to only 1 instruction. These differences are related to the difference between the supported PTX shapes and the shapes that the SASS can work on it. For example, in Table III’s first row, the PTX instruction can use many shapes such as 16×16×16, but the SASS can only work on 16×8×16. So, 2 SASS instructions are needed to iterate over the PTX shape. However, the physical TC implementation can perform 8\*4\*8 [21]. While it is previously mentioned in [25] that the TC latencies are shape-dependent for Turing, we found that different shapes for the same data type do not affect the calculated latency. It can vary from one type to another in Ampere architecture. Our observations for the TC throughput and latencies shown in the table are consistent with the behavior mentioned in the white paper [11]. Finally, We noticed that for all half floating precision (fp16 and bf16) inputs, SASS instruction *MOVMA.16.MT88* is used for loading a matrix to the TC. In general, the *MOVMA* SASS instruction is used to move a matrix with a transpose. The number of issued *MOVMA* instructions depends on the matrix shape and the layout (row or column

major). For example, if we used A and B matrices as row major in the PTX code, then the *MOVMA* instructions are used to transpose the B matrix to multiply each row from A with each column from B. However, when we use both as Column major, the *MOVMA* instruction is used with the A and C matrices. It transposes A and C before execution and transposes C after the execution. Finally, if A is a row-major and B is a column-major, the *MOVMA* instruction does not exist in the trace. We used the same way motioned above for the latency calculations to calculate the memories throughput. The observations are quite similar to the throughput values mentioned in the white paper.

TABLE IV  
THE MEMORY ACCESSES LATENCIES

Memory type	CPI (cycles)
Global memory	290
L2 cache	200
L1 cache	33
Shared Memory (ld/st)	(23/19)

## VI. CONCLUSION

This paper demystifies the instructions, memories, and tensor cores for Nvidia Ampere architecture. We perform a detailed analysis of the PTX instructions latency while showing their SASS translation. The presented microbenchmarks are portable and can be extended for future architectures. In addition, we pointed out the microarchitecture instructions of the tensor cores and their latencies for all data types supported by the Ampere architecture. Finally, we calculate the memory latency while building the pointer chasing method for both global memory and L2 cache. This work can help in understating the hardware from the microarchitecture point of view, leading to better-optimized applications and workloads.

TABLE V  
INSTRUCTIONS CLOCK CYCLES FOR THE (Ameperre A100) GPU

PTX	SASS	cycles	PTX	SASS	cycles
<b>Add / sub instruction</b>			<b>Min/Max instructions</b>		
add.u16	UIADD3	2	Min.u16	ULOP3.LUT+UISETP.LT.U32.AND+USEL	8
addc.u32	IADD3.X	2	min.u32	IMNMX.U32	2
add.u32	IADD	2	min.u64	UISETP.LT.U32.AND+2*USEL	8
add.u64	UIADD3.x+ UIADD3	4	min.s16	PRMT+IMNMX	4
add.s64	UIADD3.x+UIADD3	4	min.s32	IMNMX	2
add.f16	HADD	2	Min.s64	UISETP.LT.U32.AND+UISETP.LT.AND.EX+2*USEL	8
add.f32	FADD	2	min.f16	HMNMX2+PRMT	4
add.f64	DADD	4	min.f32	FMNMX	2
<b>Mul instruction</b>			min.f364	DSETP.MIN.AND+IMAD.MOV.U32+UMOV+FSEL	10
mul.wide.u16	LOP3.LUT+IMAD	4	<b>Neg instruction</b>		
mul.wide.u32	IMAD	4	neg.s16	UIADD3+UPRMT	5
mul.lo.u16	LOP3.LUT+IMAD	4	neg.s32	IADD3	2
mul.lo.u32	IMAD	2	neg.s64	IMAD.MOV.U32+HFMA2.MMA+MOV+UIADD3	10
mul.lo.u64	IMAD	2	neg.f32	FADD or IMAD.MOV.U32 *	2
mul24.lo.u32	PRMT + IMAD	3	neg.f64	DADD+(UMOV)	4
mul24.hi.u32	UPRMT+USHF.R.U32.HI+IMAD.U32+PRMT	9	<b>FMA instruction</b>		
mul.rn.f16	HMUL2	2	fma.rn.f16	HFMA2	2
mul.rn.f32	FMUL	2	fma.rn.f32	FFMA	2
mul.rn.f64	DMUL	4	fma.rn.f64	DFMA	4
<b>MAD Instruction</b>			<b>Sqrt Instruction</b>		
mad.lo.u16	LOP3.LUT+IMAD	4	sqrtn.f32	[multiple instrs including MUFU.RSQ]	190-235
mad.lo.u32	FFMA	2	sqrtn.approx.f32	[multiple instrs including MUFU.SQRT]	2-18
mad.lo.u64	IMAD	2	sqrtn.f64	[multiple instrs including MUFU.RSQ64]	260-340
mad24.lo.u32	SGXT.U32 + IMAD	4	<b>Rsqrt Instruction</b>		
mad24.hi.u32	USHF.R.U32.HI+UIMAD.WIDE.U32+2*UPRMT+IADD3	11	rsqrtn.approx.f32	[multiple instrs including MUFU.RSQ]	2-18
mad.rn.f32	FFMA	2	rsqrtn.approx.f64	MUFU.RSQ64H	8-11
mad.rn.f64	DFMA	4	<b>Rcp Instruction</b>		
<b>Sad Instruction</b>			rcp.rn.f32	[multiple instrs including MUFU.RCP]	198
sad.u16/s16	(2*LOP3) +UOP3+ VABSDIFF	6	rcp.approx.f32	[multiple instrs including MUFU.RCP]	23
sad.u32/s32	VABSDIFF +IMAD (1 IMAD + 1 Umov for 3 instrs)	3	rcp.rn.f64	[multiple instrs including MUFU.RCP64H]	244
sad.u64/s64	UISETP.GE.U32.AND+UIADD+IADD	10	ex2.approx.f32	FSTEP + FMUL + MUFU.EX2 + FMUL	14
<b>Div / Rem Instruction</b>			<b>Pop Instruction</b>		
rem/div.u16/s16	multiple instructions	290	popc.b32S	POPC	6
rem/div.s32/u32	multiple instructions	66	popc.b64	2*UPOPC + UIADD3	7
rem/div.u64/s64	multiple instructions	420	<b>Clz Instruction</b>		
div.rn.f32	multiple instructions	525	clz.b32	FLO.U32 + IADD	7
div.rn.f64	multiple instructions	426	clz.b64	UISETP.NE.U32.AND+USEL+UFLO.U32+2*UIADD3	13
<b>Abs Instruction</b>			<b>Bfind Instruction</b>		
abs.s16	PRMT+IABS+PRMT	4	bfind.u32	FLO.U32	6
abs.s32	IABS	2	bfind.u64	FLO.U32+ISETP.NE.U32.AND+IADD3+BRA	164
abs.s64	UISETP.LT.AND+UIADD3.X +UIADD3+2*USEL	11	bfind.s32	FLO	6
abs.f16	PRMT	1	bfind.s64	multiple instructions	195
abs.ftz.f32	FADD.FTZ	2	<b>testp Instruction</b>		
abs.f64	DADD or (DADD+UMOV)	4	testp.normal.f32	IMAD.MOV.U32+2*UISETP.GE.U32.AND	0 or 6
<b>Brev Instruction</b>			testp.subnor.f32	ISETP.LT.U32.AND	0 or 6
brev.b32	BREV + SGXT.U32	2	testp.normal.f64	2*UISETP.LE.U32.AND+2*UISETP.GE.U32.AND	13
brev.b64	2*UBREV+MOV	6	testp.subnor.f64	UISETP.LT.U32.AND+2*UISETP.GE.U32.AND.EX	8
<b>copysign Instruction</b>			<b>Other Instruction</b>		
copysign.f32	2*LOP3.LUT or 1.5*LOP3.LUT	4	sin.approx.f32	FMUL + MUFU.SIN	8
copysign.f64	2*UOP3.LUT+IMAD.U32+*MOV	6	cos.approx.f32	FMUL.RZ+MUFU.COS	8
<b>and/or/xor Instruction</b>			lg2.approx.f32	FSETP.GEU.AND+FMUL+MUFU.LG2+FADD	18
and.b16	LOP3.LUT or 1.5*LOP3.LUT	2	ex2.approx.f32	FSETP.GEU.AND+2*FMUL+MUFU.EX2	18
and.b32	LOP3.LUT	2	ex2.approx.f16	MUFU.EX2.F16	6
and.b64	UOP3.LUT	2-3	tanh.approx.f32	MUFU.TANH	6
<b>Not Instruction</b>			tanh.approx.f16	MUFU.TANH.F16	6
not.b16	LOP3.LUT	2	bar.warp.sync;	NOP	changes
not.b32	LOP3.LUT	2	fns.b32	multiple instructions	79
not.b64	2*UOP3.LUT	4	cvt.rzi.s32.f32	F2I.TRUNC.NTZ	6
<b>lop3 Instruction</b>			setp.ne.s32	ISETP.NE.AND	10
lop3.b32	IMAD.MOV.U32+LOP3.LUT	4	mov.u32 clock	CS2R.32	2
<b>cnot Instruction</b>			<b>Bfi Instruction</b>		
cnot.b16	UOP3.LUT+ISETP.EQ.U32.AND+SEL	5	bfi.b32	3*PRMT+2*IMAD.MOV+SHF.L.U32+BMSK+LOP3.LUT	11
cnot.b32	UISETP.EQ.U32.AND+USEL	4	bfi.b64	UMOV+USHF.L.U32+(UIADD3+UOP3.LUT)*	5
cnot.b64	multiple instructions	11	<b>dp4a.u32/s32 Instruction</b>		
<b>bfe Instruction</b>			dp4a.u32.u32	IMAD.MOV.U32+IDP.4A.U8.U8	135-170
bfe.s32/u32	3*PRMT+2*IMAD.MOV+SHF.R.U32.HI+SGXT/U32	11	<b>dp2a.u32/s32 Instruction</b>		
bfe.u64	UMOV+USHF.L.U32+(UIADD3+UOP3.LUT)*	5	dp2a.lo.u32.u32	IMAD.MOV.U32+IDP.2A.LO.U16.U8	135-170
bfe.s64	multiple instructions	14			



## REFERENCES

- [1] *Meta AI Supercomputer*, 2022. [Online]. Available: <https://ai.facebook.com/blog/ai-rsc/>
- [2] *Top500 List*. [Online]. Available: <https://www.top500.org/lists/top500/2022/06/>
- [3] X. Zhang, G. Tan, S. Xue, J. Li, K. Zhou, and M. Chen, "Understanding the gpu microarchitecture to achieve bare-metal performance tuning," in *Proceedings of the 22nd ACM SIGPLAN Symposium on Principles and Practice of Parallel Programming*, 2017, pp. 31–43.
- [4] N.-M. Ho and W.-F. Wong, "Exploiting half precision arithmetic in nvidia gpus," in *2017 IEEE High Performance Extreme Computing Conference (HPEC)*, IEEE, 2017, pp. 1–7.
- [5] D. Lustig, S. Sahasrabudhe, and O. Giroux, "A formal analysis of the nvidia ptx memory consistency model," in *Proceedings of the Twenty-Fourth International Conference on Architectural Support for Programming Languages and Operating Systems*, 2019, pp. 257–270.
- [6] H. Wong, M.-M. Papadopoulou, M. Sadooghi-Alvandi, and A. Moshovos, "Demystifying gpu microarchitecture through microbenchmarking," in *2010 IEEE International Symposium on Performance Analysis of Systems and Software (ISPASS)*, IEEE, 2010, pp. 235–246.
- [7] Z. Jia, M. Maggioni, B. Staiger, and D. P. Scarpazza, "Dissecting the nvidia volta gpu architecture via microbenchmarking," *arXiv preprint*, arXiv:1804.06826, 2018.
- [8] Z. Jia, M. Maggioni, J. Smith, and D. P. Scarpazza, "Dissecting the nvidia turing t4 gpu via microbenchmarking," *arXiv preprint*, arXiv:1804.06826, 2019.
- [9] R. van Stigt, S. N. Swatman, and A.-L. Varbanescu, "Isolating gpu architectural features using parallelism-aware microbenchmarks," in *Proceedings of the 2022 ACM/SPEC on International Conference on Performance Engineering*, 2022, pp. 77–88.
- [10] M. Andersch, J. Lucas, M. A. LvLvarez-Mesa, and B. Juurlink, "On latency in gpu throughput microarchitectures," in *2015 IEEE International Symposium on Performance Analysis of Systems and Software (ISPASS)*, IEEE, 2015, pp. 169–170.
- [11] *NVIDIA A100 Tensor Core GPU Architecture*, 2022. [Online]. Available: <https://images.nvidia.com/aem-dam/en-zz/Solutions/datacenter/nvidia-ampere-architecture-whitepaper.pdf>
- [12] *Parallel Thread Execution ISA Version 7.7*, 2022. [Online]. Available: <https://docs.nvidia.com/cuda/parallel-threadexecution/index.html#instruction-set>
- [13] Y. Arafa, A.-H. A. Badawy, G. Chennupati, N. Santhi, and S. Eidenbenz, "Low overhead instruction latency characterization for nvidia gpgpus," in *2019 IEEE High Performance Extreme Computing Conference (HPEC)*, IEEE, 2019, pp. 1–8.
- [14] V. Volkov, "A microbenchmark to study gpu performance models," in *ACM SIGPLAN Notices*, vol. 53, no. 1, pp. 421–422, 2018.
- [15] A. Bakhoda, G. L. Yuan, W. W. Fung, H. Wong, and T. M. Aamodt, "Analyzing cuda workloads using a detailed gpu simulator," in *2009 IEEE international symposium on performance analysis of systems and software*, IEEE, 2009, pp. 163–174.
- [16] M. Samadi, D. A. Jamshidi, J. Lee, and S. Mahlke, "Paraprox: Pattern-based approximation for data parallel applications," in *Proceedings of the 19th international conference on Architectural support for programming languages and operating systems*, 2014, pp. 35–50.
- [17] Y. Arafa, A.-H. Badawy, A. ElWazir, A. Barai, A. Eker, G. Chennupati, N. Santhi, and S. Eidenbenz, "Hybrid, scalable, trace-driven performance modeling of gpgpus," in *Proceedings of the International Conference for High Performance Computing, Networking, Storage and Analysis*, 2021, pp. 1–15.
- [18] Y. Arafa, A.-H. A. Badawy, G. Chennupati, N. Santhi, and S. Eidenbenz, "Ppt-gpu: Scalable gpu performance modeling," *IEEE Computer Architecture Letters*, vol. 18, no. 1, pp. 55–58, 2019.
- [19] Y. Arafa, A. ElWazir, A. ElKanishy, Y. Aly, A. Elsayed, A.-H. Badawy, G. Chennupati, S. Eidenbenz, and N. Santhi, "Verified instruction-level energy consumption measurement for nvidia gpus," in *Proceedings of the 17th ACM International Conference on Computing Frontiers*, 2020, pp. 60–70.
- [20] X. Mei and X. Chu, "Dissecting gpu memory hierarchy through microbenchmarking," *IEEE Transactions on Parallel and Distributed Systems*, vol. 28, no. 1, pp. 72–86, 2016.
- [21] W. Sun, A. Li, T. Geng, S. Stuijk, and H. Corporaal, "Dissecting tensor cores via microbenchmarks: Latency, throughput and numerical behaviors," *arXiv preprint arXiv:2206.02874*, 2022.
- [22] S. Markidis, S. W. Der Chien, E. Laure, I. B. Peng, and J. S. Vetter, "Nvidia tensor core programmability, performance & precision," in *2018 IEEE international parallel and distributed processing symposium workshops (IPDPSW)*, IEEE, 2018, pp. 522–531.
- [23] M. Fasi, N. J. Higham, M. Mikaitis, and S. Pranesh, "Numerical behavior of nvidia tensor cores," *PeerJ Computer Science*, vol. 7, p. e330, 2021.
- [24] N. Bombieri, F. Busato, F. Fummi, and M. Scala, "Mipp: A microbenchmark suite for performance, power, and energy consumption characterization of gpu architectures," in *2016 11th IEEE Symposium on Industrial Embedded Systems (SIES)*, IEEE, 2016, pp. 1–6.
- [25] M. A. Raihan, N. Goli, and T. M. Aamodt, "Modeling deep learning accelerator enabled gpus," in *2019 IEEE International Symposium on Performance Analysis of Systems and Software (ISPASS)*, IEEE, 2019, pp. 79–92.
- [26] D. Yan, W. Wang, and X. Chu, "Demystifying tensor cores to optimize half-precision matrix multiply," in *2020 IEEE International Parallel and Distributed Processing Symposium (IPDPS)*, IEEE, 2020, pp. 634–643.
- [27] M. V. Kothiya et al, "Understanding the isa impact on gpu architecture," 2014.
- [28] *NVIDIA CUDA programming. User's guide*, 2022. [Online]. Available: <https://docs.nvidia.com/cuda/cuda-c-programming-guide/index.html>